

























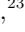








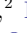











Uncovering a Massive $z \sim 7.65$ Galaxy Hosting a Heavily Obscured Radio-Loud QSO Candidate in COSMOS-Web

ERINI LAMBRIDES ^{1,*} MARCO CHIABERGE ^{2,3} ARIANNA S. LONG ^{4,†} DAIZHONG LIU ⁵ HOLLIS B. AKINS ⁴
ANDREW F. PTAK ¹ IRHAM TAUFIK ANDIKA ^{6,5} ALESSANDRO CAPETTI ⁷ CAITLIN M. CASEY ^{4,8}
JACLYN B. CHAMPAGNE ⁹ KATHERINE CHWOROWSKY ^{4,‡} OLIVIA R. COOPER ^{4,‡} XUHENG DING ¹⁰
ANDREAS L. FAISST ¹¹ MAXIMILIEN FRANCO ⁴ STEVEN GILLMAN ^{8,12} GHASSEM GOZALIASL ^{13,14}
KIRSTEN R. HALL ¹⁵ SANTOSH HARISH ¹⁶ CHRISTOPHER C. HAYWARD ¹⁷ MICHAELA HIRSCHMANN ^{18,19}
TAYLOR A. HUTCHISON ^{1,*} KNUD JAHNKE ²⁰ SHUOWEN JIN ^{8,21,§} JEYHAN S. KARTALTEPE ¹⁶
ANTON M. KOEKEMOER ²² VASILY KOKOREV ²³ SINCLAIRE M. MANNING ^{24,†} CRYSTAL L. MARTIN ²⁵
JED MCKINNEY ⁴ COLIN NORMAN ^{2,3} MASAFUSA ONOUE ^{26,10} BRANT E. ROBERTSON ²⁷ MARKO SHUNTOV ^{28,29}
JOHN D. SILVERMAN ^{30,31} MASSIMO STIAVELLI ² BENNY TRAKHTENBROT ³² ELENI VARDOLAKI ³³
JORGE A. ZAVALA ³⁴ NATALIE ALLEN ^{28,29} OLIVIER ILBERT ³⁵ HENRY JOY MCCrackEN ³⁶
LOUISE PAQUEREAU ³⁶ JASON RHODES ³⁷ AND SUNE TOFT ^{28,29}

¹NASA-Goddard Space Flight Center, Code 662, Greenbelt, MD, 20771, USA

²Space Telescope Science Institute, 3700 San Martin Drive Baltimore, MD 21218, USA

³Department of Physics & Astronomy, Johns Hopkins University, Bloomberg Center, 3400 N. Charles St., Baltimore, MD 21218, USA

⁴Department of Astronomy, The University of Texas at Austin, 2515 Speedway Blvd Stop C1400, Austin, TX 78712, USA

⁵Max-Planck-Institut für Astrophysik, Karl-Schwarzschild-Str. 1, D-85748 Garching, Germany

⁶Technical University of Munich, TUM School of Natural Sciences, Department of Physics, James-Frank-Str. 1, D-85748 Garching, Germany

⁷INAF Osservatorio Astrofisico di Torino, Strada Osservatorio 20, I10025 Pino Torinese, Italy

⁸Cosmic Dawn Center (DAWN), Denmark

⁹Steward Observatory, University of Arizona, 933 N Cherry Ave, Tucson, AZ 85721, USA

¹⁰Kavli Institute for the Physics and Mathematics of the Universe (Kavli IPMU, WPI), The University of Tokyo, Chiba 277-8583, Japan

¹¹Caltech/IPAC, MS 314-6, 1200 E. California Blvd. Pasadena, CA 91125, USA

¹²DTU-Space, Technical University of Denmark, Elektrovej 327, DK-2800 Kgs. Lyngby, Denmark

¹³Department of Computer Science, Aalto University, P. O. Box 15400, Espoo, FI-00076, Finland

¹⁴Department of Physics, University of Helsinki, P. O. Box 64, FI-00014, Helsinki, Finland

¹⁵Radio & Geoastronomy Division, Center for Astrophysics | Harvard & Smithsonian, 60 Garden St. Cambridge, MA 02138, USA

¹⁶Laboratory for Multiwavelength Astrophysics, School of Physics and Astronomy, Rochester Institute of Technology, 84 Lomb Memorial Drive, Rochester, NY 14623, USA

¹⁷Center for Computational Astrophysics, Flatiron Institute, 162 Fifth Avenue, New York, NY 10010, USA

¹⁸Institute of Physics, GalSpec, Ecole Polytechnique Federale de Lausanne, Observatoire de Sauverny, Chemin Pegasi 51, 1290 Versoix, Switzerland

¹⁹INAF, Astronomical Observatory of Trieste, Via Tiepolo 11, 34131 Trieste, Italy

²⁰Max Planck Institute for Astronomy, Königstuhl 17, D-69117 Heidelberg, Germany

²¹DTU-Space, Technical University of Denmark, Elektrovej 327, 2800 Kgs. Lyngby, Denmark

²²Space Telescope Science Institute, 3700 San Martin Dr., Baltimore, MD 21218, USA

²³Kapteyn Astronomical Institute, University of Groningen, PO Box 800, 9700 AV Groningen, The Netherlands

²⁴Department of Astronomy, University of Massachusetts Amherst, MA 01003, USA

²⁵Department of Physics, University of California, Santa Barbara, Santa Barbara, CA 93109, USA

²⁶Kavli Institute for Astronomy and Astrophysics, Peking University, Beijing 100871, China

²⁷Department of Astronomy and Astrophysics, University of California, Santa Cruz, 1156 High Street, Santa Cruz, CA 95064, USA

²⁸Cosmic Dawn Center (DAWN), Copenhagen, Denmark

²⁹Niels Bohr Institute, University of Copenhagen, Jagtvej 128, DK-2200, Copenhagen, Denmark

³⁰Kavli Institute for the Physics and Mathematics of the Universe (WPI), The University of Tokyo, Kashiwa, Chiba 277-8583, Japan

³¹Department of Astronomy, School of Science, The University of Tokyo, 7-3-1 Hongo, Bunkyo, Tokyo 113-0033, Japan

³²School of Physics and Astronomy, Tel Aviv University, Tel Aviv 69978, Israel

³³Thüringer Landessternwarte, Sternwarte 5, 07778 Tautenburg, Germany

³⁴National Astronomical Observatory of Japan, 2-21-1 Osawa, Mitaka, Tokyo 181-8588, Japan

³⁵Aix Marseille Univ, CNRS, CNES, LAM, Marseille, France

³⁶Institut d'Astrophysique de Paris, UMR 7095, CNRS, and Sorbonne Université, 98 bis boulevard Arago, F-75014 Paris, France

³⁷Jet Propulsion Laboratory, California Institute of Technology, 4800 Oak Grove Drive, Pasadena, CA 91001, USA

ABSTRACT

In this letter, we report the discovery of the highest redshift, heavily obscured, radio-loud QSO candidate selected using JWST NIRCам/MIRI, mid-IR, sub-mm, and radio imaging in the COSMOS-Web field. Using multi-frequency radio observations and mid-IR photometry, we identify a powerful, radio-loud (RL), growing supermassive black hole (SMBH) with significant spectral steepening of the radio SED ($f_{1.32\text{GHz}} \sim 2$ mJy, $q_{24\mu\text{m}} = -1.1$, $\alpha_{1.32-3\text{GHz}} = -1.2$, $\Delta\alpha = -0.4$). In conjunction with ALMA, deep ground-based observations, ancillary space-based data, and the unprecedented resolution and sensitivity of JWST, we find no evidence of QSO contribution to the UV/optical/NIR data and thus infer heavy amounts of obscuration ($N_H > 10^{23} \text{ cm}^{-2}$). Using the wealth of deep UV to sub-mm photometric data, we report a singular solution photo- z of $z_{\text{phot}} = 7.65^{+0.4}_{-0.3}$ and estimate an extremely massive host-galaxy ($\log M_* = 11.92 \pm 0.06 M_\odot$). This source represents the furthest known obscured RL QSO candidate, and its level of obscuration aligns with the most representative but observationally scarce population of QSOs at these epochs.

1. INTRODUCTION

Recent discoveries of $z > 6$ extremely powerful ($L_{\text{Bol}} \sim 10^{46} \text{ erg s}^{-1}$) active galactic nuclei (hereinafter referred to as QSOs) have launched intense debate as to how such massive black holes ($\sim 10^9 M_\odot$) can form so early in the Universe (Mortlock et al. 2011; Bañados et al. 2018; Inayoshi et al. 2020; Wang et al. 2021). Questions surrounding the triggering and growth of these QSOs have largely remained unanswered. This is driven by the fact that almost all direct observations of $z > 6$ QSOs are *unobscured* – the very energy that makes these sources detectable at high-redshifts overwhelms the star-forming (SF) contributions from their host galaxies in rest-frame UV–NIR imaging.

Thus it is paramount to observe powerful QSO at $z > 6$ whose central engines are heavily obscured for the following reasons: (1) Unlike with unobscured QSOs, the host galaxy properties of obscured QSOs (e.g., M_* , morphology) are more accessible in regimes where the QSO emission is significantly attenuated (i.e., rest-frame UV/optical); (2) According to a combination of theory and observations over 80% of QSOs are expected to be heavily obscured ($N_H > 10^{23} \text{ cm}^{-2}$) by their host-galaxies at $z > 6$, and over 99% by $z > 7$ (Ni et al. 2020; Gilli et al. 2022). The obscuration of AGN can occur over a vast range of physical scales and conditions.

In the local Universe, obscured QSO are contextualized by the standard sight-line dependent unification scheme – where the dominant source of obscuration is thought to occur a few parsecs from the accretion disk by an optically thick toroidal or cloud structure and exhibit a lack of intrinsic difference between the host-galaxy and BH properties of their unobscured QSO counterparts (Antonucci 1993; Urry & Padovani 1995). New evidence is accumulating that at higher redshifts, the dominant sources of QSO obscuration may exist on kpc scales (Circosta et al. 2019; D’Amato et al. 2020). In both theory and observations, it is shown that at increasing redshifts, galaxies are clumpy and less settled (Faure et al. 2021; Kartaltepe et al. 2023), and have higher ISM densities (Buchner et al. 2017; Dalton et al. 2021; Gilli et al. 2022). Therefore, it is unsurprising that recent studies find high QSO obscured fractions due to the increased chances of UV/optical photons from the accretion disk being significantly attenuated along its path through its host galaxy (Ni et al. 2020; Gilli et al. 2022).

Recent JWST spectroscopic and photometric observations have yielded a litany of $z > 5$ actively accreting SMBHs (Kocevski et al. 2023; Larson et al. 2023; Labbe et al. 2023; Matthee et al. 2023; Furtak et al. 2023; Maiolino et al. 2023), yet for these sources – some of which are heavily reddened – their rest-frame UV–Optical emission probes their QSO nature, and thus by definition are not heavily obscured. Even JWST/MIRI spectra of $z \sim 7$ QSOs probe rest-frame $\lesssim 2\mu\text{m}$ emission (i.e. Bosman et al. 2023), and for the most obscured AGN, their nature may only be robustly revealed at

* NPP Fellow

† NASA Hubble Fellow

‡ NSF Graduate Research Fellow

§ Marie Curie Fellow

rest mid-infrared (MIR) wavelengths in lieu of sufficient detection of high-ionization lines (Hickox & Alexander 2018). Thus, these newly measured JWST sources may not represent the most common type of QSO at these epochs, and it is yet to be determined whether their formation and/or evolution is intrinsically different from the high- z obscured QSO population. From black hole seeds to QSO feedback, the interpretation of JWST discovered high- z QSO candidates may be significantly impacted if there are different triggering pathways or host-galaxy properties of obscured vs. unobscured AGN.

Despite the predicted increased number density of high- z heavily obscured QSOs, their identification is incredibly difficult due to their heavy obscuration at wavelengths shorter than the MIR and lack of observing facilities that are capable of probing the rest-frame MIR at these epochs. Rest-frame optical-NIR spectroscopy will lack the characteristic broad lines evident in unobscured sources and requires careful analysis of multiple, well-detected narrow lines to constrain whether the source of the ionizing photons is dominated by AGN vs. star-forming processes (Onoue et al. 2021). In addition, X-ray facilities are generally incapable of reaching the sensitivities required for other than a handful of sources at $z = 6-7$ (Vito et al. 2019) and a potentially lensed $z = 10$ source (Bogdan et al. 2023; Goulding et al. 2023). On the other hand, radio emissions can penetrate through dense columns of gas and dust, and current facilities can reach the required sensitivities. Still, QSOs that exhibit a significant excess of *non-thermal* radio emission above what would be expected from star-formation and thermal AGN contribution alone (defined as Radio-Loud; RL) are rare ($< 10\%$ of the total QSO population, Kellermann et al. 1989; Herrera Ruiz et al. 2018).

Interestingly, a powerful, heavily obscured radio source ($L_{\text{Bol}} \sim 10^{46} \text{ erg s}^{-1}$) was discovered at $z \sim 7$ (COS-87259, Endsley et al. 2022) – and even this object posed more questions than it answered. COS-87259, first identified in the COSMOS field thanks to the broad bandwidth and depths accessed in the COSMOS survey, was recently spectroscopically confirmed at $z = 6.8$ via [CII] detection in ALMA Band 6 observations (Endsley et al. 2023). Bona fide evidence of the central engine in COS-87259 was discovered due to its bright radio emission. At $z \sim 7$, space density estimates of UV-bright sources are estimated to be $1/3000 \text{ deg}^2$ (Shen et al. 2020), and for RL QSOs, $1/5000 \text{ deg}^2$ (Ighina et al. 2023) – yet this source was found in a HSC 1.5 deg^2 survey.

Current UV-based absorption-corrected space density estimates imply that 10% of the cosmic black hole

growth in the Universe occurred by $z = 6$ with a rapid build-up of growth occurring between $z = 4$ and 2 (Shen et al. 2020; Matsuoka et al. 2023). Increasing the number density of obscured sources above $z = 6$ inspires several nuanced questions: Is there a significant reshaping of the gas distribution in QSO host galaxies that rapidly occurs between $z = 7$ and 6? Are the UV bright QSOs a much smaller tail of a larger QSO population – and thus, our understanding of the number density estimates and accretion history of SMBHs over cosmic time needs to be overhauled? It is difficult to answer these questions when only one heavily obscured QSO at $z \sim 7$ has been identified, i.e., COS-87259.

In this letter, we report the discovery of COSW-106725 in the COSMOS-Web field. This source was initially detected in the NIR (UVISTA + HST WFC3IR), Radio (VLA + VLBA), and sub-mm (ALMA 343 GHz continuum). During the April 2023 JWST Cycle 1 COSMOS-Web program observations, 4 NIRCam + 1 MIRI bands were imaged. Section 2 describes the observations of X-ray to sub-mm data of the source. Section 3 reports the results from SED fitting and describes the derived QSO and galaxy properties. Section 4 compares the source to the only similar source on record and contextualizes these findings regarding high- z obscured QSO demographics. In Section 4, we present the summary and conclusion. We use an $h = 0.7$, $\Omega_m = 0.3$, $\Omega_\Lambda = 0.7$ cosmology throughout this paper.

2. MULTI-WAVELENGTH OBSERVATIONS OF COSW-106725

The target was first erroneously classified over 10 years ago during a search for low-luminosity radio galaxies at cosmic noon within the COSMOS field (COSMOS-FRI-07, see Chiaberge et al. 2009 for details). COSMOS is a deep, wide area, multi-wavelength survey centered on RA +150.2688161, Dec +2.0343093 (Scoville et al. 2007). Extensive observations of the field from almost all major space- and ground-based telescopes have accrued over the past 20 years (Laigle et al. 2016; Weaver et al. 2022). The initial basic selection criteria of Chiaberge et al. (2009) was based on the initial COSMOS multi-wavelength catalog (Capak et al. 2007) and initial VLA 1.4 GHz observations (Bondi et al. 2008). This required the radio flux (at 1.4 GHz) to be between 1 and 13 mJy and the optical magnitude to be higher than $i + 21$ (Vega). Although COSW-106725 made the initial sample selection in the radio range, the source was erroneously associated with the combined optical detections of a bright star and a lower- z interloper within $2''$ of the radio coordinates. The initial NIR (CFHT) and

Table 1. Multi-wavelength ground- and space-based photometry for COSW-106725. All upper limits are at the 3σ level.

Band	Flux (μJy)
Subaru/HSC <i>g</i>	< 0.021
Subaru/HSC <i>r</i>	< 0.034
Subaru/HSC <i>i</i>	< 0.043
HST/WFC3 <i>F814W</i>	< 0.048
Subaru/HSC <i>z</i>	< 0.063
Subaru/HSC <i>y</i>	< 0.093
JWST/NIRCam <i>F115W</i>	0.092 ± 0.002
JWST/NIRCam <i>F150W</i>	0.21 ± 0.009
HST/WFC3 <i>F160W</i>	0.22 ± 0.011
JWST/NIRCam <i>F277W</i>	1.0 ± 0.09
<i>Spitzer</i> /IRAC 3.6 μm	3.05 ± 0.4
JWST/NIRCam <i>F444W</i>	5.34 ± 0.05
<i>Spitzer</i> /IRAC 4.5 μm	5.5 ± 0.49
<i>Spitzer</i> /IRAC 5.8 μm	7.71 ± 0.57
JWST/MIRI <i>F770W</i>	11.0 ± 1.33
<i>Spitzer</i> /MIPS 24 μm	91.3 ± 27.2
<i>Herschel</i> /PACS 100 μm	< 0.012
<i>Herschel</i> /PACS 160 μm	$< 2.2 \times 10^5$
<i>Herschel</i> /SPIRE 250 μm	$< 1.8 \times 10^5$
<i>Herschel</i> /SPIRE 350 μm	$< 1.6 \times 10^5$
<i>Herschel</i> /SPIRE 500 μm	$< 9.7 \times 10^{-4}$
JCMT/SCUBA-2 850 μm	$< 2.6 \times 10^3$
ALMA 343 GHz	$2.5 \times 10^3 \pm 5 \times 10^4$
VLA 3 GHz	$0.776 \times 10^3 \pm 0.04 \times 10^4$
VLA 1.4 GHz	$1.78 \times 10^3 \pm 0.15 \times 10^4$
MeerKAT 1.32 GHz	$1.99 \times 10^3 \pm 8.8$
VLA 324 MHz	$6.27 \times 10^3 \pm 0.48 \times 10^4$

MIR (*Spitzer*/IRAC) (Sanders et al. 2007) fluxes were also highly uncertain due to poor spatial resolution and multiple interlopers. The limiting spatial resolution of the optical-MIR data and the discordance between the radio and the source’s optical properties were noted, and the nature of the object was left unknown.

In the past ten years, deeper imaging and new wavelength coverage have been taken in the COSMOS field. In addition to deeper radio data, larger radio coverage, and a growing number of ALMA observations – the central 0.54 deg^2 of the COSMOS field was chosen for the largest JWST program scheduled for observations during the observatory’s first cycle in both sky coverage and total prime time allocation (COSMOS-Web Survey, PID #1727, PIs: Kartaltepe & Casey; Casey et al. 2022). COSMOS-Web consists of one large contiguous

0.54 deg^2 NIRCcam mosaic conducted in four filters, with additional MIRI imaging covering 0.18 deg^2 , and will be completed by January 2024. Within the current 0.27 deg^2 covered, this combination of new data in the COSMOS field has lifted the veil of uncertainty around COSW-106725 – and allowed us to identify the highest-redshift heavily obscured radio-loud QSO candidate to date. In the following sub-sections, we highlight the relevant observations conducted since the initial discovery of COSW-106725.

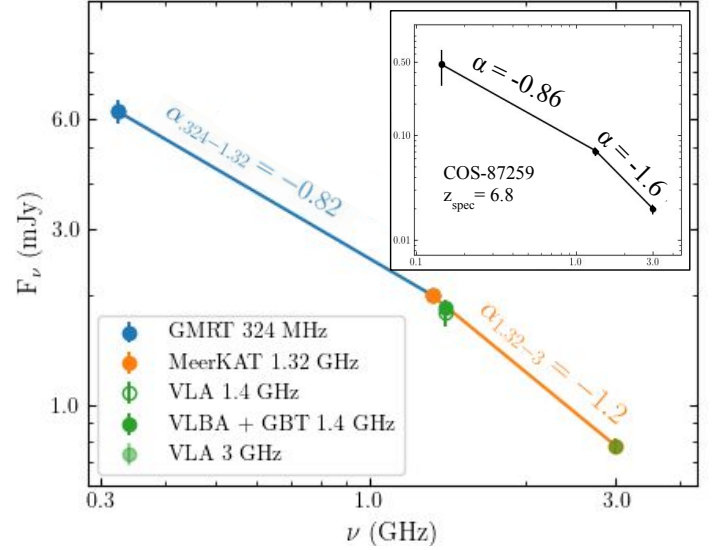


Figure 1. Radio SED: All fluxes and associated errors are listed in Table 1. We measure the spectral slope between two sets of radio frequencies (blue line, orange line) and find significant spectral steepening indicative of high- z RL QSO (Saxena et al. 2018a; Endsley et al. 2022; Broderick et al. 2022). In the upper-right corner inset, we show the radio SED for the $z_{\text{spec}} = 6.8$ heavily obscured RL AGN from Endsley et al. 2022 for reference.

2.1. Radio

The COSMOS field has been observed over a large range of radio wavelengths (325 MHz–3 GHz) via the Very Large Array (VLA), Very Long Baseline Array (VLBA), and the Giant Metrewave Radio Telescope (GMRT) (Smolčić et al. 2014). COSW-106725 was strongly detected with GMRT 324 MHz ($6.27 \pm 0.480 \text{ mJy}$) (Smolčić et al. 2014), MeerKAT 1.32 GHz ($1.99 \pm 8.8 \times 10^{-3} \text{ mJy}$) (Hale et al. 2023), VLA 1.4 GHz ($1.78 \pm 0.15 \text{ mJy}$) (Bondi et al. 2008), VLBA 1.4 GHz ($1.84 \pm 0.1 \text{ mJy}$) (Herrera Ruiz et al. 2018), and VLA 3 GHz ($0.776 \pm 0.04 \text{ mJy}$) (Smolčić et al. 2017). The physical extent of the VLA 3 GHz detection deconvolved with the beam is $< 2.2''$.

In Figure 1, we plot the radio SED of COSW-106725. Using $S_\nu \propto \nu^\alpha$, we measure the radio slope between 324 MHz and 1.32 GHz ($\alpha_{324-1.32} = -0.82$) and the radio slope between 1.32 GHz and 3 GHz ($\alpha_{1.32-3} = -1.2$). This spectral steepening toward higher frequencies is consistent not only with the reported radio properties of COS-87259 but also with the behavior of many spectroscopically confirmed $z > 4$ RL QSOs (Miley & De Breuck 2008; Saxena et al. 2018b; Yamashita et al. 2020; Drouart et al. 2020; Broderick et al. 2022).

Finally, we compare the *Spitzer* MIPS 24 μ m and VLA 1.4 GHz fluxes to assess the level of non-thermal AGN contribution to the radio emission. The observed 24 μ m and 1.4 GHz fluxes are tightly related for thermal sources (i.e. non-RL AGN and star-forming galaxies). Using the parametrization in Bonzini et al. (2013), we measure the value of $q_{24\text{obs}} = \log_{10}(f_{24\mu\text{m}}/f_{1.4\text{GHz}}) = -1.1$, indicating the presence of powerful radio emission due to a kpc-scale jetted AGN or compact radio source vs thermal emission associated with radio-quiet AGN and/or star-formation.

2.2. ALMA

COSW-106725 has a robust 5σ detection ($F_{\text{int}} = 2.5 \pm 0.5$ mJy) in $\sim 870 \mu\text{m}$ band continuum imaging via the A3COSMOS catalog (Liu et al. 2019). The A3COSMOS catalog used the rich public Atacama Large Millimeter/Submillimeter Array (ALMA) archive to generate automated mining pipelines across the COSMOS field. We use the Gaussian fit flux via the “blind” pipeline. We note the “prior”-fitting photometry catalog yields an equivalent flux measurement (see Liu et al. (2019) for details).

2.3. X-ray

The source was previously covered with the Chandra ACIS-I detector (160 ks, Civano et al. 2016a) and the XMM-Newton PN, MOS1, and MOS2 detections (30 ks, Cappelluti et al. 2009). This source is un-detected in the Chandra-Legacy survey of the COSMOS field and the XMM-COSMOS survey (Civano et al. 2016b; Cappelluti et al. 2009). We calculate the upper-limit 2–10 keV flux in the 160 ks combined event image using the CIAO tools function `aprates` (Fruscione et al. 2006), and find $F_{2-10\text{keV}} < 2.3 \times 10^{15} \text{ erg s}^{-1} \text{ cm}^{-2}$. In Section 4, we further discuss the X-ray upper-limits.

2.4. Additional Ground and Space-Based Optical/NIR/MIR Imaging

All optical upper limits are drawn from the “classic” COSMOS2020 catalog (Weaver et al. 2022). Included in COSMOS2020 is ultra-deep, broad-band photometry from the second public data release of the Hyper

Suprime-Cam (HSC) Subaru Strategic Program comprising the g , r , i , z , and y bands. COSW-106725 is undetected in all bands (g : $\text{mag}_{\text{lim}} = 28.1$, r : $\text{mag}_{\text{lim}} = 27.8$, i : $\text{mag}_{\text{lim}} = 27.6$, z : $\text{mag}_{\text{lim}} = 27.2$, and y : $\text{mag}_{\text{lim}} = 26.5$). HST/ACS $F814W$ high-resolution photometry is also included, and the object remains undetected ($\text{mag}_{\text{lim}} = 27.8$).

A search of COSW-106725’s radio coordinates in MAST serendipitously finds a WFC3IR F160W image of another source covered in an unrelated HST campaign (PI: Conselice, Cycle 24, GO:14721). Using Source Extractor (Bertin & Arnouts 1996) on the MAST reduced image, we measure a $1''$ aperture $F160W$ flux that agrees with the JWST $F150W$ flux. This source is also detected in all four *Spitzer* IRAC bands and MIPS 24 μ m. We use the source locations in the JWST NIRCam $F277W$ and radio bands to deblend the *Spitzer* photometry and find excellent photometric agreement with JWST NIRCam $F444W$ and IRAC Ch 2 (see Jin et al. 2018 for details).

The positional accuracy of the radio, ALMA, and JWST emission are all within $1''$. All fluxes and upper limits are listed in Table 1.

2.5. JWST NIRCam+MIRI Imaging

This object is in the Cycle 1 JWST COSMOS-Web field (GO #1727, PIs: Kartaltepe & Casey, Casey et al. 2022), with observations available in four NIRCam wide-band filters: $F115W$, $F150W$, $F277W$, and $F444W$, and one MIRI wide-band filter: $F770W$. Forthcoming papers will comprehensively describe the complete data reduction process (COSMOS-Web NIRCam; M. Franco et al., COSMOS-Web MIRI; S. Harish et al.), but we briefly outline the procedures here. Upon retrieval of the uncalibrated NIRCam images from the STScI MAST Archive, we reduced the data utilizing the JWST Calibration Pipeline (Bushouse et al. 2022). Custom modifications were incorporated, such as mitigating $1/f$ noise and subtracting low-level background, following the precedent set by other JWST studies (e.g., Bagley et al. 2023). All reference files, including in-flight data, represented the latest calibrations available during our observations. The final mosaics were generated during Stage 3 of the pipeline, varying only in resolution, with pixel sizes of $0.03''/\text{pixel}$ and $0.06''/\text{pixel}$. Unless otherwise specified, we will refer to the $0.06''/\text{pixel}$ resolution mosaic hereafter. The JWST mosaics were aligned to a version of the COSMOS F814W mosaic (Koekemoer et al. 2007) that had been astrometrically aligned to Gaia DR3, with the F814W mosaic subsequently used as a reference catalog for all the JWST imaging (Koekemoer et al. 2007).

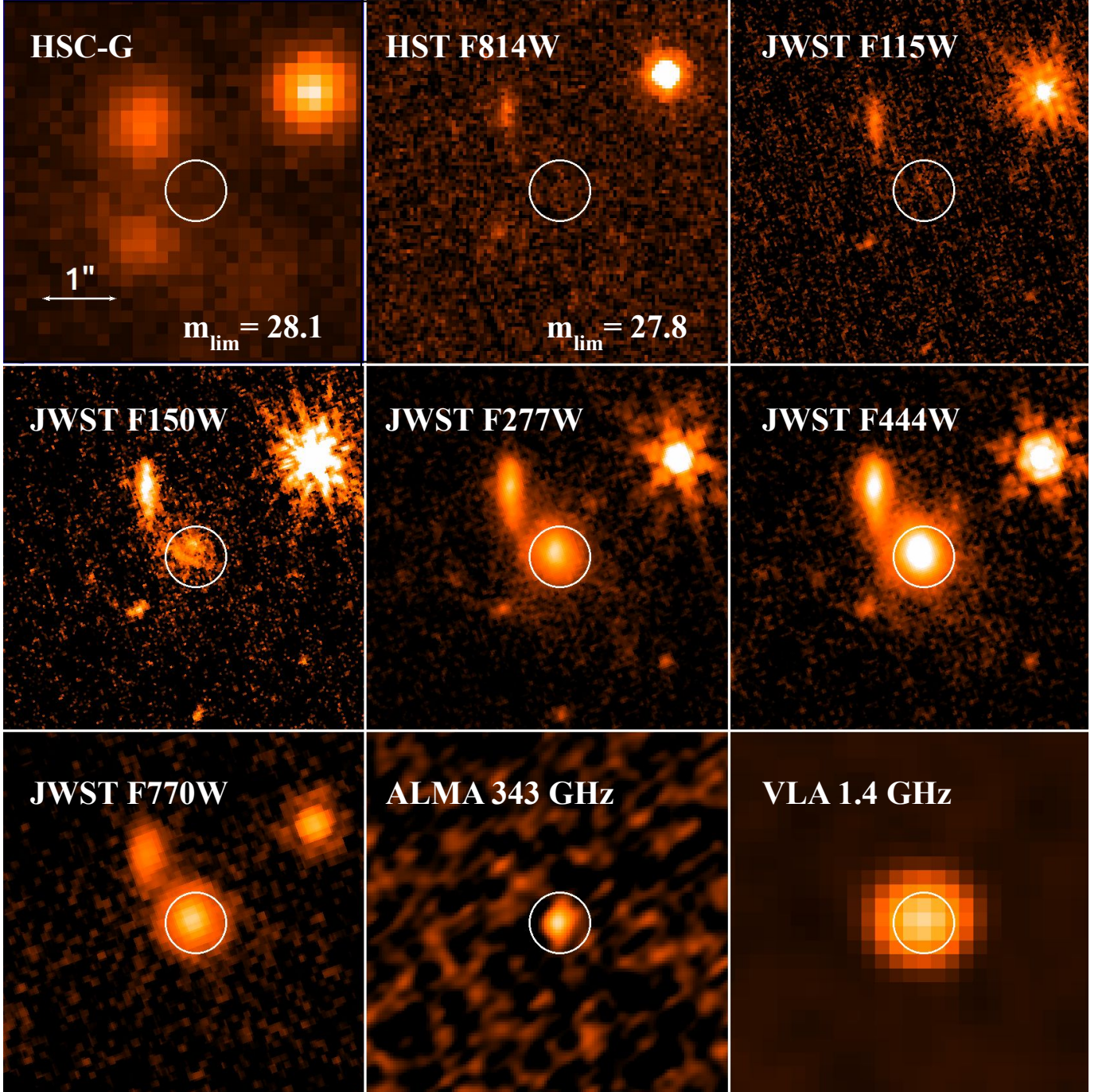


Figure 2. Selection of Postage Stamp Images of the Candidate $z \sim 7.65$ RL Quasar, COSW-106725. Top row, from left to right: HSC- g , ACS $F814W$, JWST $F115W$, JWST $F150W$, JWST $F277W$ and, JWST $F444W$, JWST MIRI $F770W$, ALMA 343 GHz and VLA 1.4 GHz. The ALMA extent is overlaid on each image (in white). The 3σ upper-limits are reported for the non-detections. The upper left source in the UV/Optical/NIR images is a low- z interloper [Weaver et al. \(2022\)](#).

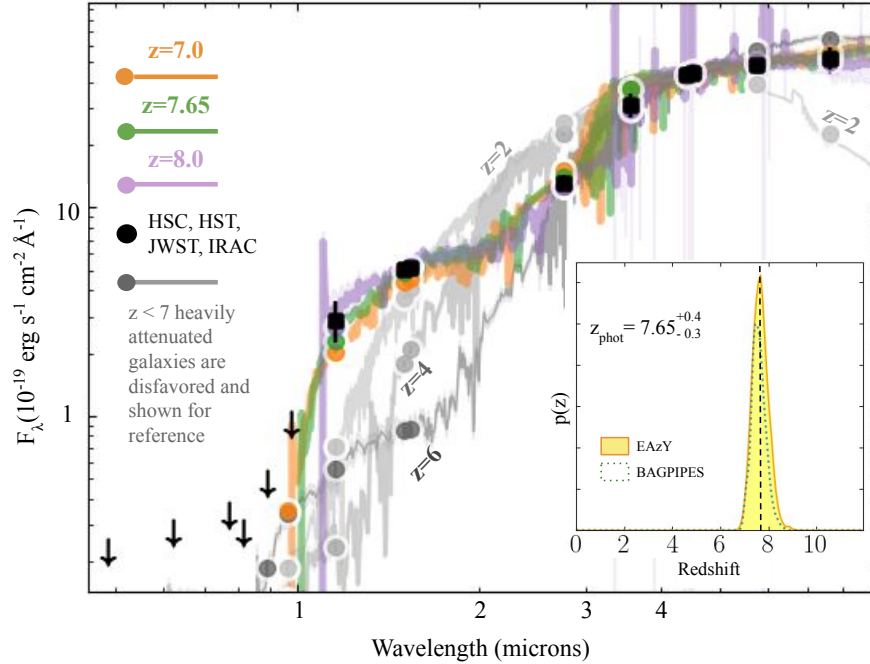


Figure 3. Results from fitting the optical, NIR and MIR with *EaZy*. Non-detections with 27 mag upper limits: HSC *g*, HSC *r*, HSC *i*, HSC *z*, HST *F814W*, HSC *y*. $> 3\sigma$ detections: JWST *F115W*, JWST *F150W*, HST *F160W*, JWST *F277W*, IRAC Channel 1, JWST *F444W*, IRAC Channel 2, IRAC Channel 3, JWST MIRI 7.7 μm . The redshift is constrained to $z = 7.65^{+0.4}_{-0.3}$ fit with combinations of SSP template from (Bruzual & Charlot 2003). Inset: We show the $p(z)$ via EAzy and BAG

The median offset between the *F814W* mosaic and the COSMOS-Web NIRCcam mosaic is less than 5 mas.

The MIRI *F770W* observations were also reduced using the JWST Calibration pipeline and with the additional background subtraction step to mitigate instrumental effects. The *F770W* mosaic was then resampled to an output grid corresponding to $0.06''/\text{pixel}$ and aligned with the HST ACS *F814W* imaging. We perform source detection and measure the multi-wavelength aperture photometry of the COSMOS-Web data using Source Extractor V 2.86 (SE, Bertin & Arnouts 1996). We use $1''$ apertures and apply a detection threshold corresponding to a signal-to-noise ratio (S/N) of 3.

3. RESULTS

3.1. Photo- z Estimate via Optical/NIR/MIR Photometry

With the photometry listed in Table 1, we first run EAzy, a template-based SED fitting code (Brammer et al. 2008). EAzy generates a photo- z probability density function (PDF) via χ^2 minimization using linear combinations of pre-defined templates. We use the standard 12 template FSPS set included in EAzy (tweak_fspqs_QSF_12.v3) and the 6 additional templates from Larson et al. 2022. In conjunction with the deep ground-based data and the unprecedented resolution and sensitivity of JWST – we perform robust SED fit-

ting on the source and find a singular solution photo- z estimate of $z_{\text{phot}} = 7.65^{+0.4}_{-0.3}$ with reduced $\chi^2 = 0.3$.

The Balmer break spectral region is well sampled with IRAC+JWST observations, and the Lyman break is sampled via deep HSC/HST+JWST observations. The detection level in *F115W* places a strict $z < 8$ constraint. In Figure 3, we also show (gray lines) the fits to templates of heavily dust-obscured star-forming galaxies at $z < 7$. The HST *F160W* + JWST *F150W*/*F277W* detections heavily disfavor any templates with $2 < z < 7$ while the MIRI *F770W* detection solidly rules out the $z \geq 2$ templates. The IRAC data used in the fit well samples the data as is evidenced by the similar fluxes in IRAC Ch 2 ($4.5 \mu\text{m}$) and JWST *F444W* ($4.4 \mu\text{m}$). In addition to the fit photo- z , the ancillary observations of this source robustly constrain the redshift to within $z = 7-8$.

We also independently measure the photo- z using BAGPIPES using a delayed-tau star-formation history ($\log(M_*/M_\odot) \sim 6-13$, $Z \sim 0.001-2.5$, $\tau \sim 0.1-5$ Gyr, Age $\sim 0-100\%$ t_H), constant starburst (Age $\sim 1-100$ Myr), nebular emission ($\log U \sim -4$ to -1), flexible dust attenuation law ($A_V \sim 0-3$, slope allowed to vary with a Gaussian prior centered on an SMC dust law), and redshift ($z \sim 0-12$). We find a consistent photo- z ($z = 7.5 \pm 0.35$, $\chi^2 = 0.27$), $A_V \sim 2$, and a $M_* = 2.8-5.4 \times 10^{11} M_\odot$. In Figure 3, we overlay the BAGPIPES $p(z)$ in the lower-left inset.

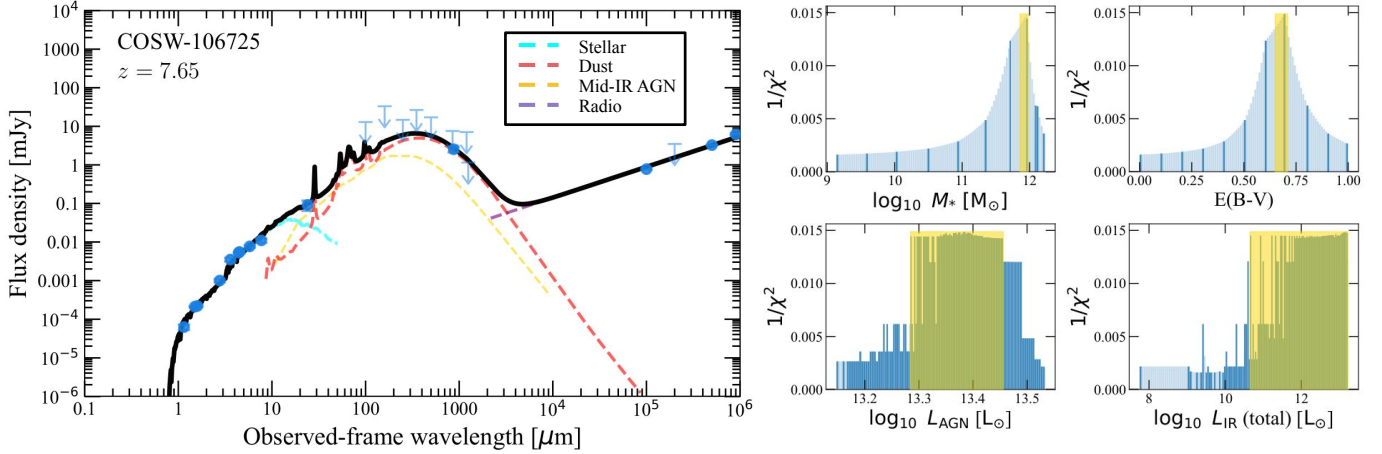


Figure 4. *Left Panel:* Optical-IR-radio SED fitting with BC03 stellar (Bruzual & Charlot 2003), mid-IR AGN (Mullaney et al. 2011), Draine & Li dust (Draine & Li 2007) and power-law radio templates (using the MICH2 code; (Liu et al. 2021)). The black line indicates the composite best-fit model and the blue symbols are photometric data points, with upper limits shown as downward arrows. The stellar, mid-IR AGN, dust, and radio components are indicated by the cyan, yellow, red, and magenta dashed lines, respectively. *Right panels:* The $1/\chi^2$ distributions from the fitting for the four parameters: stellar mass, dust attenuation $E(B - V)$, QSO component’s luminosity integrated over 10-1000 μm , and dust component’s luminosity integrated over 8-1000 μm . The yellow highlighted regions correspond to the 95% confidence intervals.

3.2. SED Decomposition at Best-Fit Photo- z

Using the photo- z derived via EAZY, we then fit the global optical-IR-radio SED with a composite of SED components accounting for stars, mid-IR AGN, dust, and radio emission to produce tighter constraints on the stellar mass and infer the QSO bolometric luminosity (Fig. 4). We use the MICH2 code¹ to fit multiple SED components simultaneously: a) the BC03 (Bruzual & Charlot 2003) synthesized stellar templates (with a constant star formation history and Calzetti et al. 2010 attenuation law), b) the low-redshift observationally-constructed mid-IR AGN templates (Mullaney et al. 2011), c) the widely-used Draine & Li dust models (Draine & Li 2007), and d) a power-law radio component with a spectral index 0.8, consistent for most radio-loud AGN (Smolčić et al. 2017).

The best-fit SED shows a strong contribution from the AGN in the mid-IR, dominating the 20–200 μm emission. The $1/\chi^2$ distributions representing the parameter probabilities are shown in the right panels of Fig. 4. These show a well constrained stellar mass $\sim 10^{11.92 \pm 0.06} M_{\odot}$, dust attenuation of $E(B - V) \sim 0.68 \pm 0.03$, and a loosely constrained dust infrared luminosity $\sim 10^{12} L_{\odot}$ (which has the QSO contribution subtracted).

The fitted QSO luminosity integrated over 10–1000 μm is $\sim 1\text{--}3 \times 10^{13} L_{\odot}$, corresponding to an QSO

bolometric luminosity of $\sim 4\text{--}12 \times 10^{46} \text{ erg s}^{-1}$ via the bolometric correction provided in Delvecchio et al. (2014). The bolometric luminosity of the source, coupled with the lack of any point source in the NIR images and lack of detection in the Chandra-Legacy 160 ks survey, allows us to infer the level of obscuration of the QSO to be $N_H > 10^{23} \text{ cm}^{-2}$. Given that this quasar is heavily obscured in the optical, we do not include a rest-frame UV-optical quasar template in our fitting.

Next, we compare the above SED-derived L_{Bol} to the L_{Bol} estimated from the X-ray upper limit. We apply the correction provided in Duras et al. (2020) to estimate the hard-band X-ray luminosity from the bolometric luminosity derived via SED fitting and calculate: $L_{2\text{--}10\text{keV, SED}} = 2\text{--}10 \times 10^{44} \text{ erg s}^{-1}$. We then calculate the X-ray 2–10 keV luminosity using the X-ray flux upper-limit derived in Section 2.3 and the photo- z estimated from Section 3.1, and find $L_{2\text{--}10\text{keV, X-ray}} < 1.5 \times 10^{45} \text{ erg s}^{-1}$. Thus, assuming this object is at $z = 7.65$, the bolometric luminosity derived from the optical-sub-mm SED fit agrees with the X-ray-based upper limit estimate.

4. DISCUSSION AND CONCLUSIONS

Assuming Eddington accretion, $\lambda_{\text{Edd}} = 1$, we provide a lower limit to the black-hole mass of COSW-106725. Following the canonical Eddington luminosity relationship using $L_{\text{Bol}} = 5.1 \times 10^{46} \text{ erg s}^{-1}$, we find $M_{\text{BH}} \geq 6.4 \times 10^8 M_{\odot}$. While this number is only a lower limit, we can calculate whether COSW-106725 is potentially more massive than expected by comparing the M_*

¹ <https://github.com/1054/Crab.Toolkit.michi2>; (Liu et al. 2021)

derived from the SED fit in Section 3.2 to the M_* derived from local M_{BH} vs. M_* scaling relations. Using Equation 8 from Ding et al. 2020, we find that the comparable stellar mass for this black hole mass should be $M_* = 3.69 \times 10^{11} M_\odot$. Due to the M_{BH} being a lower limit, the scaling relation derived M_* is also a lower limit and is below the SED fit derived M_* value ($8.3 \times 10^{11} M_\odot$). Thus, our estimated M_{BH} does not indicate an over-massive BH concerning its host galaxy.

In summary, we report the discovery of COSW-106725 in the COSMOS-Web field. The coincident radio/sub-mm/JWST observations of the source provide a robust estimate of $z_{\text{phot}} = 7.65$. This source is first detected in the rest-frame optical via JWST *F115W* and remains undetected in deep space- and ground-based $0.4\text{--}1\text{ }\mu\text{m}$ imaging. Due to the high-inferred $L_{\text{Bol}} = 5.1 \times 10^{46} \text{ erg s}^{-1}$ and lack of QSO evidence in the optical/NIR/X-ray, the source is inferred to be heavily obscured ($N_{\text{H}} > 10^{23} \text{ cm}^{-2}$). The detection of this source (COSW-106725) and COS-87259 (Endsley et al. 2023) within the epoch of $z = 6.8\text{--}8$ in a 1.5 deg^2 field hints that the space density of luminous, radio-loud QSOs at these epochs may be underestimated by over a factor of 2000. Even in the local Universe, radio-loud QSOs are only a subset of the total QSO population ($< 10\%$) and at $z = 7$ up to now have had a measured space density of $1/5000 \text{ deg}^2$ (Ighina et al. 2023). Thus, the discovery of two radio-loud, heavily obscured QSOs within 1.5 deg^2 at $z \sim 7$ is at the intersection of increasing improbability (Ighina et al. 2023).

For there to be more QSOs in the Epoch of Reionization than predicted via extrapolation of luminosity functions at lower redshifts, a very rapid change in the gas properties of QSO host galaxies must occur (Vito et al. 2018). Selecting heavily obscured sources at high redshift remains challenging even with JWST, and answering the nuanced questions surrounding early BH formation and growth with sparse data sets is challenging. Thus, combining JWST imaging with deep radio data can potentially revolutionize our understanding of powerful, obscured sources at cosmic dawn by enabling their efficient selection.

Acknowledgments: We will thank the anonymous referees for their thoughtful insight and important contributions to this work. ELL and TAH are supported by appointment to the NASA Postdoctoral Program (NPP) at NASA Goddard Space Flight Center, administered by Oak Ridge Associated Universities under contract with NASA. We acknowledge the extensive use of the following Python packages:

Software: pandas, scipy, ipython, matplotlib (McKinney 2010; Virtanen et al. 2020; Pérez & Granger 2007; Hunter 2007, respectively). This research used **astropy**, a community-developed core Python package for Astronomy (Astropy Collaboration et al. 2013).

REFERENCES

- Antonucci, R. 1993, ARA&A, 31, 473, doi: [10.1146/annurev.aa.31.090193.002353](https://doi.org/10.1146/annurev.aa.31.090193.002353)
- Astropy Collaboration, Robitaille, T. P., Tollerud, E. J., et al. 2013, A&A, 558, A33, doi: [10.1051/0004-6361/201322068](https://doi.org/10.1051/0004-6361/201322068)
- Bañados, E., Venemans, B. P., Mazzucchelli, C., et al. 2018, Nature, 553, 473, doi: [10.1038/nature25180](https://doi.org/10.1038/nature25180)
- Bagley, M. B., Finkelstein, S. L., Koekemoer, A. M., et al. 2023, ApJL, 946, L12, doi: [10.3847/2041-8213/acbb08](https://doi.org/10.3847/2041-8213/acbb08)
- Bertin, E., & Arnouts, S. 1996, A&AS, 117, 393, doi: [10.1051/aas:1996164](https://doi.org/10.1051/aas:1996164)
- Bogdan, A., Goulding, A., Natarajan, P., et al. 2023, arXiv e-prints, arXiv:2305.15458, doi: [10.48550/arXiv.2305.15458](https://doi.org/10.48550/arXiv.2305.15458)
- Bondi, M., Ciliegi, P., Schinnerer, E., et al. 2008, ApJ, 681, 1129, doi: [10.1086/589324](https://doi.org/10.1086/589324)
- Bonzini, M., Padovani, P., Mainieri, V., et al. 2013, MNRAS, 436, 3759, doi: [10.1093/mnras/stt1879](https://doi.org/10.1093/mnras/stt1879)
- Bosman, S. E. I., Álvarez-Márquez, J., Colina, L., et al. 2023, arXiv e-prints, arXiv:2307.14414, doi: [10.48550/arXiv.2307.14414](https://doi.org/10.48550/arXiv.2307.14414)
- Brammer, G. B., van Dokkum, P. G., & Coppi, P. 2008, ApJ, 686, 1503, doi: [10.1086/591786](https://doi.org/10.1086/591786)
- Broderick, J. W., Drouart, G., Seymour, N., et al. 2022, PASA, 39, e061, doi: [10.1017/pasa.2022.42](https://doi.org/10.1017/pasa.2022.42)
- Bruzual, G., & Charlot, S. 2003, MNRAS, 344, 1000, doi: [10.1046/j.1365-8711.2003.06897.x](https://doi.org/10.1046/j.1365-8711.2003.06897.x)
- Buchner, J., Schulze, S., & Bauer, F. E. 2017, MNRAS, 464, 4545, doi: [10.1093/mnras/stw2423](https://doi.org/10.1093/mnras/stw2423)
- Bushouse, H., Eisenhamer, J., Dencheva, N., et al. 2022, JWST Calibration Pipeline, 1.8.2, Zenodo, Zenodo, doi: [10.5281/zenodo.7325378](https://doi.org/10.5281/zenodo.7325378)
- Calzetti, D., Wu, S. Y., Hong, S., et al. 2010, ApJ, 714, 1256, doi: [10.1088/0004-637X/714/2/1256](https://doi.org/10.1088/0004-637X/714/2/1256)
- Capak, P., Aussel, H., Ajiki, M., et al. 2007, ApJS, 172, 99, doi: [10.1086/519081](https://doi.org/10.1086/519081)

- Cappelluti, N., Brusa, M., Hasinger, G., et al. 2009, AAP, 497, 635, doi: [10.1051/0004-6361/200810794](https://doi.org/10.1051/0004-6361/200810794)
- Casey, C. M., Kartaltepe, J. S., Drakos, N. E., et al. 2022, arXiv e-prints, arXiv:2211.07865, doi: [10.48550/arXiv.2211.07865](https://doi.org/10.48550/arXiv.2211.07865)
- Chiaberge, M., Tremblay, G., Capetti, A., et al. 2009, ApJ, 696, 1103, doi: [10.1088/0004-637X/696/2/1103](https://doi.org/10.1088/0004-637X/696/2/1103)
- Circosta, C., Vignali, C., Gilli, R., et al. 2019, A&A, 623, A172, doi: [10.1051/0004-6361/201834426](https://doi.org/10.1051/0004-6361/201834426)
- Civano, F., Marchesi, S., Comastri, A., et al. 2016a, ApJ, 819, 62, doi: [10.3847/0004-637X/819/1/62](https://doi.org/10.3847/0004-637X/819/1/62)
- . 2016b, ApJ, 819, 62, doi: [10.3847/0004-637X/819/1/62](https://doi.org/10.3847/0004-637X/819/1/62)
- Dalton, T., Morris, S. L., & Fumagalli, M. 2021, MNRAS, 502, 5981, doi: [10.1093/mnras/stab335](https://doi.org/10.1093/mnras/stab335)
- D’Amato, Q., Gilli, R., Vignali, C., et al. 2020, A&A, 636, A37, doi: [10.1051/0004-6361/201936175](https://doi.org/10.1051/0004-6361/201936175)
- Delvecchio, I., Gruppioni, C., Pozzi, F., et al. 2014, MNRAS, 439, 2736, doi: [10.1093/mnras/stu130](https://doi.org/10.1093/mnras/stu130)
- Ding, X., Silverman, J., Treu, T., et al. 2020, ApJ, 888, 37, doi: [10.3847/1538-4357/ab5b90](https://doi.org/10.3847/1538-4357/ab5b90)
- Draine, B. T., & Li, A. 2007, ApJ, 657, 810, doi: [10.1086/511055](https://doi.org/10.1086/511055)
- Drouart, G., Seymour, N., Galvin, T. J., et al. 2020, PASA, 37, e026, doi: [10.1017/pasa.2020.6](https://doi.org/10.1017/pasa.2020.6)
- Duras, F., Bongiorno, A., Ricci, F., et al. 2020, A&A, 636, A73, doi: [10.1051/0004-6361/201936817](https://doi.org/10.1051/0004-6361/201936817)
- Endsley, R., Stark, D. P., Lyu, J., et al. 2022, arXiv e-prints, arXiv:2206.00018, <https://arxiv.org/abs/2206.00018>
- . 2023, MNRAS, 520, 4609, doi: [10.1093/mnras/stad266](https://doi.org/10.1093/mnras/stad266)
- Faure, B., Bornaud, F., Fensch, J., et al. 2021, MNRAS, 502, 4641, doi: [10.1093/mnras/stab272](https://doi.org/10.1093/mnras/stab272)
- Fruscione, A., McDowell, J. C., Allen, G. E., et al. 2006, in Society of Photo-Optical Instrumentation Engineers (SPIE) Conference Series, Vol. 6270, Society of Photo-Optical Instrumentation Engineers (SPIE) Conference Series, ed. D. R. Silva & R. E. Doxsey, 62701V, doi: [10.1117/12.671760](https://doi.org/10.1117/12.671760)
- Furtak, L. J., Labbé, I., Zitrin, A., et al. 2023, arXiv e-prints, arXiv:2308.05735, doi: [10.48550/arXiv.2308.05735](https://doi.org/10.48550/arXiv.2308.05735)
- Gilli, R., Norman, C., Calura, F., et al. 2022, A&A, 666, A17, doi: [10.1051/0004-6361/202243708](https://doi.org/10.1051/0004-6361/202243708)
- Goulding, A. D., Greene, J. E., Setton, D. J., et al. 2023, arXiv e-prints, arXiv:2308.02750, doi: [10.48550/arXiv.2308.02750](https://doi.org/10.48550/arXiv.2308.02750)
- Hale, C. L., Whittam, I. H., Jarvis, M. J., et al. 2023, MNRAS, 520, 2668, doi: [10.1093/mnras/stac3320](https://doi.org/10.1093/mnras/stac3320)
- Herrera Ruiz, N., Middelberg, E., Deller, A., et al. 2018, A&A, 616, A128, doi: [10.1051/0004-6361/201832969](https://doi.org/10.1051/0004-6361/201832969)
- Hickox, R. C., & Alexander, D. M. 2018, ARA&A, 56, 625, doi: [10.1146/annurev-astro-081817-051803](https://doi.org/10.1146/annurev-astro-081817-051803)
- Hunter, J. D. 2007, Computing In Science & Engineering, 9, 90, doi: [10.1109/MCSE.2007.55](https://doi.org/10.1109/MCSE.2007.55)
- Ighina, L., Caccianiga, A., Moretti, A., et al. 2023, MNRAS, 519, 2060, doi: [10.1093/mnras/stac3668](https://doi.org/10.1093/mnras/stac3668)
- Inayoshi, K., Visbal, E., & Haiman, Z. 2020, Annual Review of Astronomy and Astrophysics, 58, 27, doi: [10.1146/annurev-astro-120419-014455](https://doi.org/10.1146/annurev-astro-120419-014455)
- Jin, S., Daddi, E., Liu, D., et al. 2018, ApJ, 864, 56, doi: [10.3847/1538-4357/aad4af](https://doi.org/10.3847/1538-4357/aad4af)
- Kartaltepe, J. S., Rose, C., Vanderhoof, B. N., et al. 2023, ApJL, 946, L15, doi: [10.3847/2041-8213/acad01](https://doi.org/10.3847/2041-8213/acad01)
- Kellermann, K. I., Sramek, R., Schmidt, M., Shaffer, D. B., & Green, R. 1989, AJ, 98, 1195, doi: [10.1086/115207](https://doi.org/10.1086/115207)
- Kocevski, D. D., Onoue, M., Inayoshi, K., et al. 2023, arXiv e-prints, arXiv:2302.00012, doi: [10.48550/arXiv.2302.00012](https://doi.org/10.48550/arXiv.2302.00012)
- Koekemoer, A. M., Aussel, H., Calzetti, D., et al. 2007, ApJS, 172, 196, doi: [10.1086/520086](https://doi.org/10.1086/520086)
- Labbe, I., Greene, J. E., Bezanson, R., et al. 2023, arXiv e-prints, arXiv:2306.07320, doi: [10.48550/arXiv.2306.07320](https://doi.org/10.48550/arXiv.2306.07320)
- Laigle, C., McCracken, H. J., Ilbert, O., et al. 2016, ApJS, 224, 24, doi: [10.3847/0067-0049/224/2/24](https://doi.org/10.3847/0067-0049/224/2/24)
- Larson, R. L., Hutchison, T. A., Bagley, M., et al. 2022, arXiv e-prints, arXiv:2211.10035, doi: [10.48550/arXiv.2211.10035](https://doi.org/10.48550/arXiv.2211.10035)
- Larson, R. L., Finkelstein, S. L., Kocevski, D. D., et al. 2023, arXiv e-prints, arXiv:2303.08918, doi: [10.48550/arXiv.2303.08918](https://doi.org/10.48550/arXiv.2303.08918)
- Liu, D., Lang, P., Magnelli, B., et al. 2019, ApJs, 244, 40, doi: [10.3847/1538-4365/ab42da](https://doi.org/10.3847/1538-4365/ab42da)
- Liu, D., Daddi, E., Schinnerer, E., et al. 2021, ApJ, 909, 56, doi: [10.3847/1538-4357/abd801](https://doi.org/10.3847/1538-4357/abd801)
- Maiolino, R., Scholtz, J., Curtis-Lake, E., et al. 2023, arXiv e-prints, arXiv:2308.01230, doi: [10.48550/arXiv.2308.01230](https://doi.org/10.48550/arXiv.2308.01230)
- Matsuoka, Y., Onoue, M., Iwasawa, K., et al. 2023, ApJL, 949, L42, doi: [10.3847/2041-8213/acd69f](https://doi.org/10.3847/2041-8213/acd69f)
- Matthee, J., Naidu, R. P., Brammer, G., et al. 2023, arXiv e-prints, arXiv:2306.05448, doi: [10.48550/arXiv.2306.05448](https://doi.org/10.48550/arXiv.2306.05448)
- McKinney, W. 2010, in Proceedings of the 9th Python in Science Conference, ed. S. van der Walt & J. Millman, 51 – 56
- Miley, G., & De Breuck, C. 2008, A&A Rv, 15, 67, doi: [10.1007/s00159-007-0008-z](https://doi.org/10.1007/s00159-007-0008-z)
- Mortlock, D. J., Warren, S. J., Venemans, B. P., et al. 2011, Nature, 474, 616, doi: [10.1038/nature10159](https://doi.org/10.1038/nature10159)

- Mullaney, J. R., Alexander, D. M., Goulding, A. D., & Hickox, R. C. 2011, MNRAS, 414, 1082, doi: [10.1111/j.1365-2966.2011.18448.x](https://doi.org/10.1111/j.1365-2966.2011.18448.x)
- Ni, Y., Di Matteo, T., Gilli, R., et al. 2020, MNRAS, 495, 2135, doi: [10.1093/mnras/staa1313](https://doi.org/10.1093/mnras/staa1313)
- Onoue, M., Matsuoka, Y., Kashikawa, N., et al. 2021, ApJ, 919, 61, doi: [10.3847/1538-4357/ac0f07](https://doi.org/10.3847/1538-4357/ac0f07)
- Pérez, F., & Granger, B. E. 2007, Computing in Science and Engineering, 9, 21, doi: [10.1109/MCSE.2007.53](https://doi.org/10.1109/MCSE.2007.53)
- Sanders, D. B., Salvato, M., Aussel, H., et al. 2007, ApJS, 172, 86, doi: [10.1086/517885](https://doi.org/10.1086/517885)
- Saxena, A., Jagannathan, P., Röttgering, H. J. A., et al. 2018a, MNRAS, 475, 5041, doi: [10.1093/mnras/sty152](https://doi.org/10.1093/mnras/sty152)
- Saxena, A., Marinello, M., Overzier, R. A., et al. 2018b, MNRAS, 480, 2733, doi: [10.1093/mnras/sty1996](https://doi.org/10.1093/mnras/sty1996)
- Scoville, N., Aussel, H., Brusa, M., et al. 2007, ApJs, 172, 1, doi: [10.1086/516585](https://doi.org/10.1086/516585)
- Shen, X., Hopkins, P. F., Faucher-Giguère, C.-A., et al. 2020, MNRAS, 495, 3252, doi: [10.1093/mnras/staa1381](https://doi.org/10.1093/mnras/staa1381)
- Smolčić, V., Ciliegi, P., Jelić, V., et al. 2014, MNRAS, 443, 2590, doi: [10.1093/mnras/stu1331](https://doi.org/10.1093/mnras/stu1331)
- Smolčić, V., Novak, M., Bondi, M., et al. 2017, A&A, 602, A1, doi: [10.1051/0004-6361/201628704](https://doi.org/10.1051/0004-6361/201628704)
- Urry, C. M., & Padovani, P. 1995, PASP, 107, 803, doi: [10.1086/133630](https://doi.org/10.1086/133630)
- Virtanen, P., Gommers, R., Oliphant, T. E., et al. 2020, Nature Methods, 17, 261, doi: <https://doi.org/10.1038/s41592-019-0686-2>
- Vito, F., Brandt, W. N., Yang, G., et al. 2018, MNRAS, 473, 2378, doi: [10.1093/mnras/stx2486](https://doi.org/10.1093/mnras/stx2486)
- Vito, F., Brandt, W. N., Bauer, F. E., et al. 2019, AAP, 630, A118, doi: [10.1051/0004-6361/201936217](https://doi.org/10.1051/0004-6361/201936217)
- Wang, F., Yang, J., Fan, X., et al. 2021, ApJL, 907, L1, doi: [10.3847/2041-8213/abd8c6](https://doi.org/10.3847/2041-8213/abd8c6)
- Weaver, J. R., Kauffmann, O. B., Ilbert, O., et al. 2022, ApJs, 258, 11, doi: [10.3847/1538-4365/ac3078](https://doi.org/10.3847/1538-4365/ac3078)
- Yamashita, T., Nagao, T., Ikeda, H., et al. 2020, AJ, 160, 60, doi: [10.3847/1538-3881/ab98fe](https://doi.org/10.3847/1538-3881/ab98fe)